All-optical atom surface traps implemented with one-dimensional planar diffractive microstructures

O. Alloschery, R. Mathevet, J. Weiner

IRSAMC/LCAR
Université Paul Sabatier, 118 route de Narbonne,
31062 Toulouse, France
jweiner@irsamc.ups-tlse.fr

H. J. Lezec

T. J. Watson Laboratories of Applied Physics, Caltech, Pasadena, California 91125
Centre National de la Recherche Scientifique, Paris 75794, France

Abstract: We characterize the loading, containment and optical properties of all-optical atom traps implemented by diffractive focusing with one-dimensional (1D) microstructures milled on gold films. These on-chip Fresnel lenses with focal lengths of the order of a few hundred microns produce optical-gradient-dipole traps. Cold atoms are loaded from a mirror magneto-optical trap (MMOT) centered a few hundred microns above the gold mirror surface. Details of loading optimization are reported and perspectives for future development of these structures are discussed.

© 2006 Optical Society of America

OCIS codes: 020.7010 Atomic and molecular physics.Trapping; 050.1970 Diffraction and Gratings.Diffractive Optics

References and links

1. W. Hänsel, P. Hommelhoff, T. W. Hänsch and J. Reichel, "Bose-Einstein condensation on a microelectronic chip" Nature **413**, 498-501 (2001).
2. Y-J. Wang, D. Z. Anderson, V. M. Bright, E. A. Cornell, Q. Diot, T. Kishimoto, M. Prentiss, R. A. Saravanan, S. R. Segal and S. Wu, "Atom Michelson Interferometer on a Chip Using a Bose-Einstein Condensate" Phys. Rev. Lett. **94**, 090405–1-4 (2005).
3. M Wilzbach, A. Haase, M. Schwarz, D. Heine, K. Wicker, X. Liu, K-H. Brenner, S. Groth, T. Fernholz, B. Hessmo, and J. Schmiedmayer, "Detecting neutral atomson an atom chip" Fortschr. Phys. **54**, 746-764 (2006).
4. J. J. McClelland, S. B. Hill, M. Pichler, and R. J. Celotta, "Nanotechnology with atom optics" Sci. Technol. Adv. Mater. **5**, 575-580 (2004).
5. R. Long, T. Rom, W. Hänsel, T. W. Hänsch, J. Reichel, "Long distance magnetic conveyor for precise positioning of ultracold atoms" Eur. Phys. J. D **35**, 125-133 (2005).
6. J. D. Weinstein and K. G. Libbrecht, "Microscopic magnetic traps for neutral atoms" Phys. Rev. A **52**, 4004-4009 (1995).
7. J. Reichel, W. Hänsel, and T. W. Hänsch, "Atomic Micromanipulation with Magnetic Surface Traps" Phys. Rev. Lett. **83**, 3398-33401 (1999).
8. D. Cassettari, A. Chenet, R. Folman, A. Haase, B. Hessmo, P. Krüger, T. Maier, S. Schneider, T. Calarco, and J. Schmiedmayer, "Micromanipulation of neutral atoms with nanofabricated structures" Appl. Phys. B **70**, 721-730 (2000)
9. R. Dumke, M. Volk, T. Muther, F. B. J. Buchkremer, G. Birkl, and W. Ertmer, "Micro-optical Realization of Arrays of Selectrively Addresable Dipole Traps: A Scalable Configuration for Quantum Computation with Atomic Qubits" Phys. Rev. Lett. **89**, 097903–1-4 (2002).
10. T. L. Gustavson, A. P. Chikkatur, A. E. Leanhardt, A. Gorlitz, S. Gupta, D. E. Pritchard, and W. Ketterle, "Transport of Bose-Einstein Condensates with Optical Tweezers" Phys. Rev. Lett. **88**, 020401–1-4 (2002).

11. Y. Miroshnychenko, W. Alt, I. Dotsenko, L. Forster, M. Khudaverdyan, D. Meschede, D. Schrader, and A. Rauschenbeutel, "Quantum engineering: An atom-sorting machine" Nature **442**, 151-151 (2006).

12. *Technical Digest, Integrated Photonics Research and Applications and Nanophotonics* (Optical Society of America, Washington, DC, 2006).

13. S. Eriksson, M. Trupke, H. F. Powell, D. Sahagun, C. D. J. Sinclair, E. A. Curtis, B. E. Sauer, E. A Hinds, Z. Moktadir, C. O. Gollasch, and M. Kraft, "Integrated optical components on atom chips" Eur. Phys. J. D **35**, 135-139 (2005).

14. Y. B. Ovchinnikov, "Coherent manipulation of atoms by copropagating laser beams" Phys. Rev. A **73**, 033404–1-10 (2006).

15. Details of this phenomenon are described in O. Alloschery, R. Mathevet, and J. Weiner, "All-optical atom surface traps implemented with one-dimensional planar diffractive microstructures" arXiv physics/0611092(2006).

16. The capture efficiency, as distinct from the overall loading efficiency, was determined by using selective atom fluorescence to image the Fresnel intensity pattern superimposed on the MMOT cold-atom cloud. Details of this measurement have been reported in arXiv physics/0611092(2006).

17. R. Grimm and M. Weiedemüller, "Optical Dipole Traps for Neutral Atoms" Adv. At. Mol. Phys. **42**, 95-113 (2000).

18. H. J. Lezec, A. Degiron, E. Devaux, R. A Linke, L. Martin-Moreno, F. J. Garcia-Vidal, and T. W. Ebbesen, "Beaming Light from a Subwavelength Aperture" Science **297**, 820-822 (2002).

19. G. Gay, O. Alloschery, B. Viaris de Lesegno, C. O'Dwyer, J. Weiner, and H. J. Lezec, "The optical response of nanostructured surfaces and the composite diffracted evanescent wave model" Nature Phys. **2**, 262-267 (2006).

1. Introduction

Manipulation and control of matter at the micro- nano- and atomic level has become increasingly important for the investigation of cold quantum gases [1], atom interferometry [2], quantum information processing [3] and precision positioning of atoms on or under surfaces [4, 5]. For the most part magnetic forces have been used in order to take advantage of favorable scaling laws and on-chip integration technologies as component size reduces to the micron scale [6, 7, 8]. The implementation of optical forces has proceeded more slowly because the subwavelength electro-magnetic field localisation required to achieve comparable scaling-law advantages has been more difficult to realize. Earlier work has emphasized remote, table-top preparation of optical trap arrays with subsequent projection into the closed vacuum system containing the cold atoms [9] or the use of "optical tweezers" either for long-range transport of cold-atom condensates [10] or for the sorting of individual atoms in 1D strings [11]. Recent developments in integrated- and nano-photonics [12], however have renewed interest in all-optical approaches to atom and molecule manipulation using on-chip planar architectures [13, 14]. Optical forces are of interest because of their wide applicability to atoms, molecules and clusters. They rely on electrical polarization, independent of net magnetic dipole moment, while most molecules are singlets with no net magnetic dipole in the electronic ground state. Here we report a study using planar diffractive focusing to load an elongated optical dipole trap with cold atoms from a 3-D mirror magneto-optical trap [7] oriented $100 - 500 \ \mu$m above a gold mirror surface.

2. Overall Experimental setup

Figure 1 shows a schematic of the overall setup. The MMOT, cooling and repumping near the Cs $[S_{1/2}, F=4] \rightarrow$ Cs $[P_{3/2}, F'=5]$ and the Cs $[S_{1/2}, F=3] \rightarrow$ Cs $[P_{3/2}, F'=3]$ transitions respectively, produces a cloud of cold cesium atoms several hundred microns from the gold mirror surface. The MMOT consists of four 8 mW light beams with a $1/e^2$ diameter of 1.5 cm, apertured through a 16 mm diaphragm. Detuning is $\sim -2\Gamma$ in a 15 G cm^{-1} B-field gradient. The MMOT is loaded from background Cs vapor and captures $\simeq 3 \times 10^6$ atoms with a density of $\simeq 3 \times 10^{11}$ cm^{-3} at a temperature of $\simeq 30 \ \mu$K. The surface itself is formed from a gold layer 400 nm thick evaporated onto a 25 mm square, 1 mm thick fused silica substrate. Two laser beams reflect in the horizontal $x - z$ plane while two counterpropagating beams along the
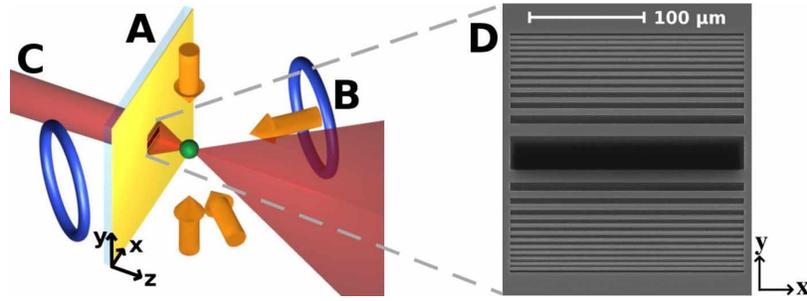
Fig. 1. Schematic of the MMOT/FFORT setup. A–Gold mirror focused-ion-beam (FIB)-milled at center with 1-D Fresnel diffraction lens. B–Laser beams and magnet coils (blue rings) forming the MMOT. Green cloud of cold Cs atoms is trapped at the MMOT center at a distance typically $100-500\,\mu$m from the mirror surface. C–Fresnel far off-resonant trap (FFORT) laser beam illuminating the mirror and Fresnel structure from the rear. D–Zoom of the Fresnel structure at the mirror center with 500 μm focal length. Overall Fresnel motif dimensions: 209 μm $\times$ 206 μm; central slit width: $\simeq$ 28 μm with 12 slits on each side. FFORT laser beam: focused gaussian TEM_{00} on the Fresnel structure with 230 μm intensity ($1/e^2$) spot diameter.
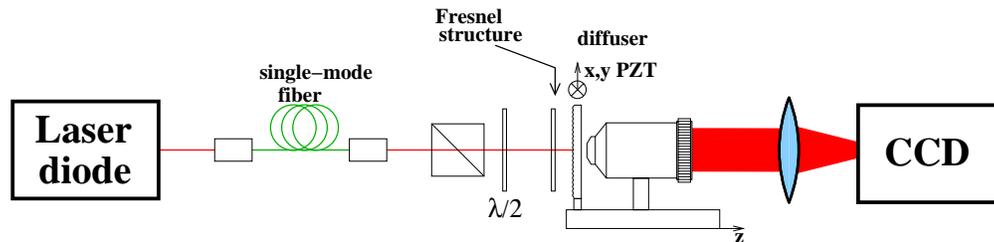

Fig. 2. Schematic of the Fresnel structure optical characterization system. The piezoelectric element dithers the diffusing screen to eliminate speckle in the spatial intensity distribution.

vertical *y* axis plus the external magnetic field gradient complete the standard six-beam MOT configuration. A focused ion beam (FIB) is used to mill at the mirror center a pattern of horizontal slits so as to produce a Fresnel diffraction lens with a 1-D focus. When illuminated from behind the mirror with an intense laser beam tuned far to the red of the Cs D2 line, the structure forms a Fresnel far-off resonance dipole trap (FFORT). To implement the FFORT we use a Ti:Sapph ring laser (Coherent 899), pumped by a 10 W, single-mode cw laser at 532 nm (Coherent Verdi). The ring laser is detuned ~ -0.5 nm from the Cs D2 resonance line with an output power of 350 mW in a diameter of 200 μm spot. This FFORT is loaded with cold atoms from the MMOT. Just prior to FFORT loading the B-field is turned off; a 1 ms molasses phase is performed while increasing the detuning to $-3\,\Gamma$ and ramping down the MMOT beam intensity. We have obtained cold Cs atom trapping using diffractive structures with focal lengths of 500 μm and 200 μm. We report here loading parameters and measured properties for the 500 μm focal-length traps.

2.1. Fresnel Lens Characterization

In order to verify the planar Fresnel lens designs we developed a separate test setup that directly measures the focal properties of these devices. Figure 2 shows the arrangement. A laser beam issuing from a stabilized laser diode coupled to a single-mode fiber is linearly polarized and
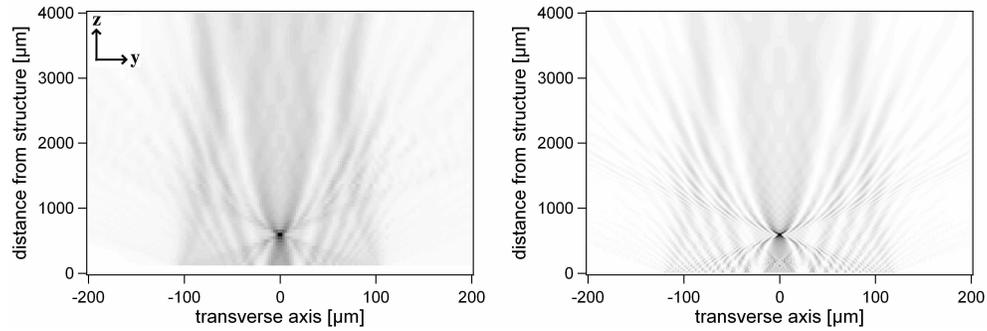
Fig. 3. Left panel: Measured spatial intensity map in the $y-z$ plane. Coordinate axes indicated in Fig. 1 and measurement setup in Fig. 2. Focal distance is designed for 500 μm. Right panel: Numerical simulation of the diffractive pattern for the structure measured in left panel.

impinges on the FIB-milled Fresnel structure from the back (substrate side). A diffuser plate placed on the output side maps the spatial intensity of the diffracted light in planes parallel to the structure plane. A piezoelectric element dithers the diffuser plate in the $x-y$ plane to eliminate the effects of speckle, and a microscope objective images the diffuser intensity pattern onto a CCD camera. The distance between the diffuser-plate-imaging-objective combination and the Fresnel structure is systematically increased along z. At each distance an image of the pattern is recorded on the CCD camera and integrated along x, the long axis of the Fresnel slits, thereby generating a series of profiles of the intensity distribution along y as a function of z. The resulting measured intensity map in the $y-z$ plane is then compared with numerical simulations to verify design accuracy. Figure 3 shows the measured profile and the numerical simulation for the 500 μm focal length Fresnel motif. The intensity profiles in the transverse focal plane and along the longitudinal axis are plotted in Fig. 4. These plots show that the simulated transverse focus profile (red curve) is significantly sharper than the measured CCD image (green curve). The black-dashed curve shows the simulated focal profile averaged over the effective spatial resolution of 2.4 μm ($\times 10$ image magnification; CCD pixel element 24 μm square). Overall dimensions of the simulated focal spot along the x, y, z directions are 192 μm, 2 μm, 35 μm, respectively. The excellent agreement between the measured profile and the spatially averaged calculated profile indicates that the red-curve simulation well represents the actual focus characteristic of the Fresnel lens. These results support and encourage the use of numerical simulations to explore more elaborate lens designs.

2.2. Atom Trap Imaging System

The atoms trapped in the MMOT and in the FFORT are imaged by an absorption profile of a probe laser beam tuned near the $F = 4 \rightarrow F' = 5$ transition. Figure 5 shows a schematic of the absorption imaging system which registers a double image: one from atom absorption followed by mirror reflection, the other from mirror reflection followed by atom absorption. We therefore obtain two projections from orthogonal directions and thus a 3D view of the atom distribution. The left panel of Fig. 6 shows a typical image of the distribution of cold atoms trapped in the MMOT when the trap center is located $\simeq 500$ μm away from the mirror surface. The optical thickness of trapped atoms in the MMOT would be sufficient to attenuate the probe laser beam almost to extinction if tuned to the absorption resonance peak. Therefore, for the MMOT images, the probe is tuned off-resonance by about four natural atomic line widths in order to maintain linearity between absorption probability and atom number. For atoms trapped
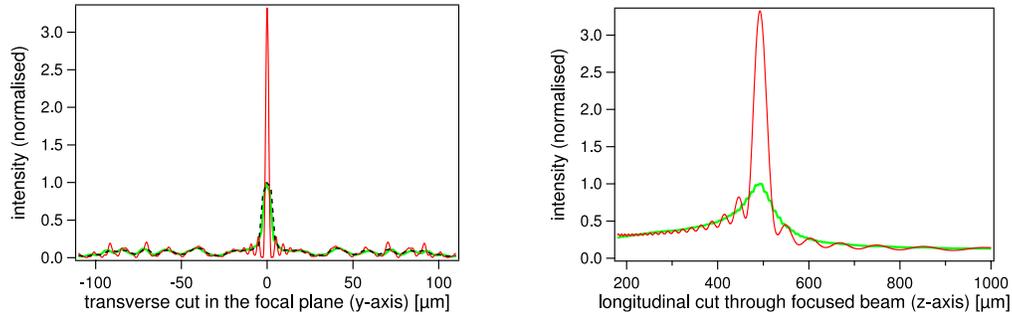
Fig. 4. Left panel: Intensity profiles in the transverse focal plane (y-axis). Red curve shows the results of the simulation in Fig. 3. Black dashed curve is the simulation averaged over the spatial resolution of the optical measurement system. Green curve is the measured intensity, normalized to unity at the peak. Right panel: Intensity profile along the longitudinal symmetry axis (z-axis). Red curve shows the numerical simulation of Fig. 3. Green curve shows the measured intensity, normalized to unity at the peak. Dimensions of the simulated focus spot (FWHM) in the x, y, z directions are are 192 μm, 2.0 μm, 35 μm, respectively.
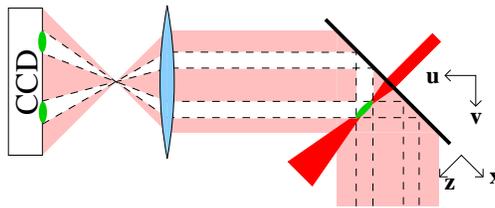

Fig. 5. Schematic of the absorption imaging system used to detect cold atoms in the MMOT and in the FORT. Green spot at focus of intense off-resonance red laser beam represents trapped atoms. Two green spots on the CCD plane represent the absorption images focused by the blue lens. Note that CCD plane is rotated by an angle of 45 degrees with respect to the mirror plane. Therefore trap images are foreshortened by $\sqrt{2}$ in the z direction.

in the FFORT, however, the imaging laser is resonant with the $F = 4 \rightarrow F' = 5$ transition. The distance from the MMOT to the mirror plane can be varied either by mechanically moving the mirror closer to the atoms with a vernier screw adjustment or by adding a bias magnetic field that translates the cloud center. The right panel of Fig. 6 shows that the minimum distance before atom loss from the trap becomes significant is $\simeq 300$ μm. We believe that the onset of this loss occurs because the vertical beams of the MMOT are partially occulted by the mirror. At the center of the mirror the resulting sharp edge diffraction produces a shadow about 100 μm wide that begins to perturb the MMOT loading rate at a comparable distance from the mirror surface.

3. FFORT atom loading from MMOT

We have carried out a series of measurements to optimize FFORT loading from the MMOT. The left panel of Fig. 7 shows an absorption image of the atoms trapped in the FFORT with 500 μm focal length. We have also investigated 200 μm focal length structures; but, in addition to atom loss from mirror proximity (see right panel Fig. 6) technical limitations associated with imaging [15], restrict systematic studies reported here to 500 μm focal-length devices.

We first measured the trapped atom number as a function of FFORT laser power. The results are shown in the right panel of Fig. 7 and, above a threshold of 20 mW, indicate a linearly
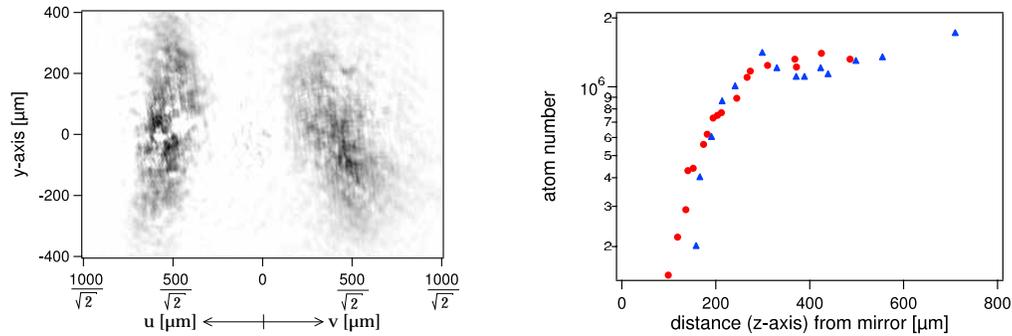
Fig. 6. Left panel: Double absorption image (see Fig. 5). Left (right) image side is the projection of atom cloud on the u-axis (v-axis), corrected by a $\sqrt{2}$ foreshortening. Right panel: Number of atoms contained in the MMOT as function of distance from the mirror surface. Blue triangles correspond to the mechanical approach (via a vernier screw translation) of the mirror surface to the MMOT, and red circles correspond to a translation of the magnetic field minimum (via a small external bias field).
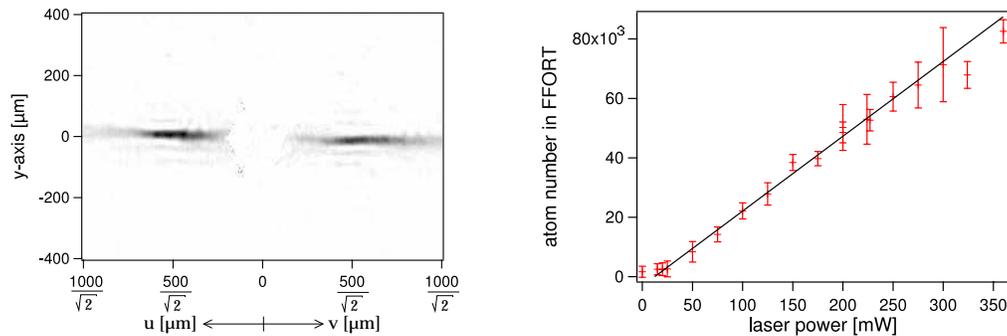

Fig. 7. Left panel: Double absorption image (see Fig. 5). Left(right) image side is the projection of atom cloud on the u-axis (v-axis), corrected by a $\sqrt{2}$ foreshortening. Image recorded 30 ms after MMOT extinction. Right panel: Atom number vs. FFORT laser power.

increasing number of atoms. As the trapping laser power grows, the effective volume of the FFORT grows as well — first in the central focal region, then in the small secondary maxima adjacent to the main peak (see Fig. 4). For these measurements the dipole-gradient trap laser detuning was fixed at $\simeq 0.5$ nm to the red of the Cs resonance line. We found that it was possible to load the lateral wings either by decreasing detuning or increasing FFORT laser power, thereby obtaining a trap of ~ 200 μm width, but only at the cost of unacceptably high rates of atom heating. It was not possible to obtain an accurate estimate of the trap depth from the incident laser power trap geometry due to uncertainties in transmission efficiency through the Fresnel structures. Unfortunately in the present setup direct *in situ* power measurement at the trap site is not technically feasible.

Next the left panel of Fig. 8 plots the atom number in the FFORT as a function of red detuning. We found that a detuning of $\simeq -0.25$ nm produced the optimum atom number. The rapid fall-off at smaller detunings is due to absorptive heating while at larger detunings it is primarily due to the inverse relation between trap depth and detuning. The data shown in Figs. 7, 8 were recorded 30 ms after extinguishing the MMOT so as to purge untrapped atoms from the imaging field of view.
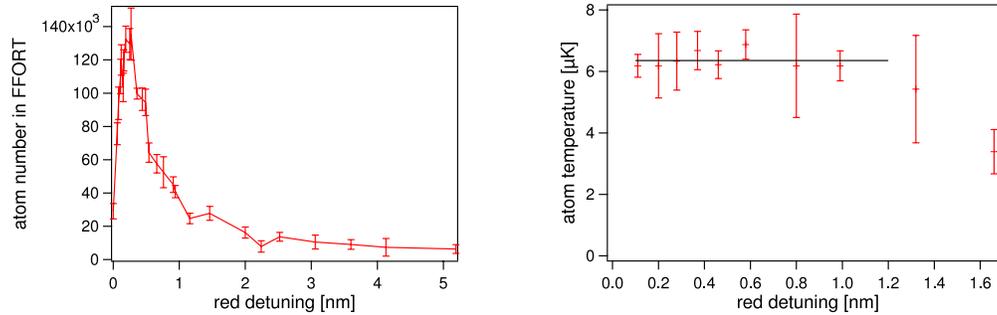
Fig. 8. Left panel: Atom number vs. FFORT detuning. Right panel: Trap temperatures vs. FFORT red detuning.

We also determined loading efficiency, defined as the ratio of trapped atoms to the initial atom number in the MMOT. The relatively poor spatial overlap between the MMOT and the FFORT (compare left panels of Figs. 6, 7), results in a rather low loading efficiency of only a few per cent. However of those atoms in the MMOT that *are* spatially overlapped by the FFORT the capture efficiency into the dipole trap approaches unity [16].

Finally we also measured the atom temperature in the confining *y* direction within the trap by monitoring the atom cloud ballistic expansion after trap release [17]. The results, as a function of trap detuning are shown in the right panel of Fig. 8. The FFORT-trapped atoms are found to be significantly colder than the atoms in the MMOT (~ 6 μK vs. ~ 30 μK). The origin of this extra cooling effect has not yet been thoroughly investigated. However from numerical simulation we estimate the trapping frequency along the confining axis to be about 13 kHz. Since a mechanical shutter extinguishes the FFORT in about 1 ms, we speculate that part of the cooling effect comes from adiabatic expansion just prior to ballistic release. Note also that the temperature starts to decline with detuning beyond ~ 1 nm, where decreasing trap depth might lead to some evaporative cooling effect.

4. Perspectives

Several different directions for development of these planar, all-optical atom trapping structures remain to be exploited. As the work presented here shows, the most promising involve not only miniaturisation but *integration* of structure functionality directly onto the chip. First, we are investigating 1D trap arrays as shown in the left and right panels of Fig. 9 and 2D arrays as well. We are also developing variable-focal-length lenses useful for capturing atoms far from the mirror and guiding them into very small volumes close to the surface. Second, we are exploring the integration of the optical structures with on-chip microelectronic circuitry and micromechanical (MEMS) devices for each array element. Dynamic addressing of the trapped cold atoms either electrically with integrated current-carrying wires or optically with laser spots provide typical examples. Finally, miniaturization can be greatly improved by reducing the size of FIB-milled Fresnel elements while maintaining adequate trapping efficiency. Further reduction to about a 10 μm footprint should be possible by taking advantage of subwavelength surface wave phenomena [18, 19]. Development of planar arrays together with atom transport and dynamic array-element addressing, opens the way to applications in quantum gate implementation and precision atom doping of surfaces.
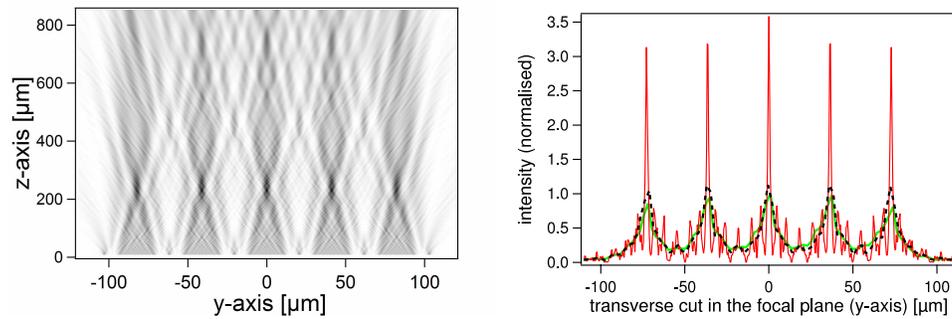
Fig. 9. Left panel: Numerical simulation of the diffractive pattern for a 1-D array of five 200 μm focal length structures measured in right panel. Right panel: Intensity profile in the transverse focal plane (y-axis) for 1D array of five 200 μm focal length lenses. Red curve shows the results of the simulation in left panel. Similar to the discussion of section 2.1, black dashed curve is the simulation averaged over the effective spatial resolution of the optical measurement system, taking into account magnification and CCD pixel size. Green curve is the measured intensity, normalized to unity at the peak.

fully acknowledged. Technical assistance and the fabrication facilities of the Caltech Kavli Nanoscience Institute are also gratefully acknowledged.